ARTICLE

Strong optomechanical coupling at room temperature by coherent scattering

Andrés de los Ríos Sommer[1], Nadine Meyer [1 ✉] & Romain Quidant [1,2,3]

Quantum control of a system requires the manipulation of quantum states faster than any decoherence rate. For mesoscopic systems, this has so far only been reached by few cryogenic systems. An important milestone towards quantum control is the so-called strong coupling regime, which in cavity optomechanics corresponds to an optomechanical coupling strength larger than cavity decay rate and mechanical damping. Here, we demonstrate the strong coupling regime at room temperature between a levitated silica particle and a high finesse optical cavity. Normal mode splitting is achieved by employing coherent scattering, instead of directly driving the cavity. The coupling strength achieved here approaches three times the cavity linewidth, crossing deep into the strong coupling regime. Entering the strong coupling regime is an essential step towards quantum control with mesoscopic objects at room temperature.

[1] ICFO-Institut de Ciencies Fotoniques, The Barcelona Institute of Science and Technology, 08860 Castelldefels (Barcelona), Spain. [2] ICREA-Institució Catalana de Recerca i Estudis Avançats, 08010 Barcelona, Spain. [3] Nanophotonic Systems Laboratory, Department of Mechanical and Process Engineering, ETH Zurich, 8092 Zurich, Switzerland. ✉email: nmeyer@ethz.ch

Laser cooling has revolutionised our understanding of atoms, ions and molecules. Lately, after a decade of experimental and theoretical efforts employing the same techniques[1–8], the motional ground state of levitated silica nanoparticles at room temperature has been reported[9]. While this represents an important milestone towards the creation of mesoscopic quantum objects, coherent quantum control of levitated nanoparticles[10,11] still remains elusive.

Levitated particles stand out among the plethora of opto-mechanical systems[12] due to their detachment, and therefore high degree of isolation from the environment. Their centre of mass, rotational and vibrational degrees of freedom[13] make them attractive tools for inertial sensing[14], rotational dynamics[15–18], free fall experiments[19], exploration of dynamic potentials[20], and are envisioned for testing macroscopic quantum phenomena at room temperature[2,10,21,22].

Recently, the centre-of-mass motion of a levitated particle has successfully been 3D cooled employing coherent scattering (CS)[8,23]. Cooling with CS is less sensitive to phase noise heating than actively driving the cavity[7,24], because optimal coupling takes place at the intensity node. Lately, this has enabled phonon occupation numbers of less than one[9].

For controlled quantum experiments, such as the preparation of non-classical, squeezed[25,26] or entangled states[27,28], the particle's motional state needs to be manipulated faster than the absorption of a single phonon from the environment. A valuable but less stringent condition is the so-called strong coupling regime (SCR), where the optomechanical coupling strength g between the mechanical motion of a particle and an external optical cavity exceeds the particle's mechanical damping Γ_m and the cavity linewidth κ ($g \gg \Gamma_m, \kappa$). The SCR presents one of the first stepping stones towards full quantum control and has been demonstrated in opto- and electromechanical systems[29–31], followed by quantum-coherent control[32].

Here, we observe normal mode splitting (NMS) in SCR with levitated nanoparticles[33], as originally reported in atoms[34]. In contrast to previous experiments, we employ CS[8,23,35,36]. Our table-top experiment offers numerous ways to tune the optomechanical coupling strength at room temperature, a working regime that is otherwise nearly exclusive to plasmonic nanocavities[37,38].

Results

Experimental setup for levitation. Our experimental setup is displayed in Fig. 1. A silica nanoparticle (green) of radius $R \approx 90$ nm, mass $m = 6.4 \times 10^{-18}$ kg and refractive index $n_r = 1.45$ is placed in a cavity (purple) by an optical tweezers trap (yellow) with wavelength $\lambda_t = 2\pi/k_t = 1064$ nm, power $P_t \simeq 150$ mW, numerical aperture NA = 0.8, and optical axis (z) perpendicular to the cavity axis (y). The trap is linearly polarised along the axis defined as $\epsilon_\theta = \epsilon_x \cos\theta$ (see inset in Fig. 1).

The nanoparticle's eigenfrequencies $\Omega_{x,y,z} = 2\pi \times (172$ kHz, 197 kHz, 56 kHz) are non-degenerate due to tight focusing. The trap is mounted on a nano-positioning stage allowing for precise 3D placement of the particle inside the low loss, high finesse Fabry-Pérot cavity with a cavity linewidth $\kappa \approx 2\pi \times 10$ kHz, cavity finesse $F = 5.4 \times 10^5$ and free spectral range $\Delta\omega_{FSR} = \pi c/L_c = 2\pi \times 5.4$ GHz. The relative detuning $\Delta = \omega_t - \omega_c$ between the trap and the cavity resonance is tunable. The intracavity photon number n_{cav} is estimated from the transmitted cavity power P_{out} (CO in Fig. 1), and the particle position displacement is measured by interfering the scattered light with a co-propagating reference beam[39]. In CS, scattering events from the detuned trapping field, locked at Δ, populate the cavity. This contrasts the approach of actively driving the cavity[3,7,24]. A particle in free space, solely
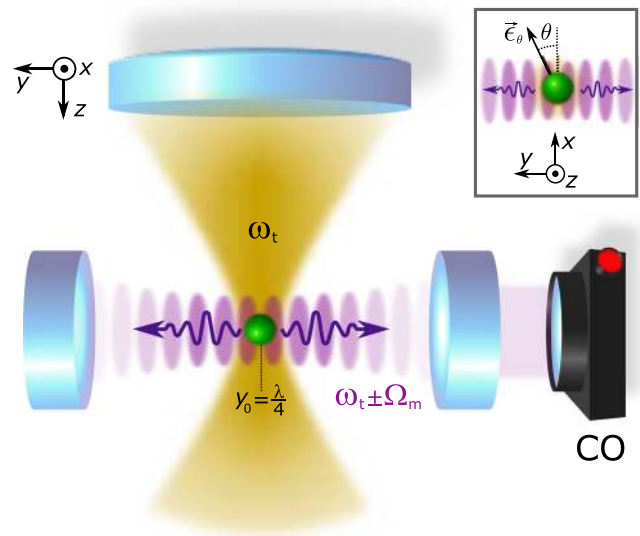
Fig. 1 Experimental setup. An optical tweezers trap (yellow) levitates a silica nanoparticle inside a high finesse cavity. The trapping field is locked relatively to the cavity resonance ω_{cav} using Pound-Drever-Hall locking with a detuning $\Delta = \omega_t - \omega_{cav}$. A 3D piezo stage positions the particle precisely inside the cavity at variable y_0. The inset displays the linear trap polarisation axis along $\epsilon_\theta = \epsilon_x \cos\theta$. The rate of coherently scattered photons into the cavity mode (purple) depends on y_0, ϵ_θ and Δ. The transmitted cavity output field is monitored on a photodiode (CO) and the forward scattered trapping light is used to detect the particle motion (see "Experimental setup" section).

interacting with the trapping light, Raman scatters photons into free space and the energy difference between incident and emitted light equals $\pm\hbar\Omega_m$ with $m = x, y, z$. In this case, photon up and down conversion are equally probable[40]. The presence of an optical cavity alters the density of states of electromagnetic modes and enhances the CS into the cavity modes through the Purcell effect. If trap photons are red (blue) detuned with respect to the cavity resonance, the cavity enhances photon up (down) conversion and net cooling (heating) takes place.

Coherent scattering theory. In order to estimate the corresponding optomechanical coupling strength in CS, we follow ref. [36]. The interaction Hamiltonian for a polarisable particle interacting with an electric field $\mathbf{E}(\mathbf{R})$ is given by $\hat{H}_{int} = -\frac{1}{2}\alpha\mathbf{E}^2(\mathbf{R})$ with the particle polarizability $\alpha = 4\pi\epsilon_0 R^3 \frac{n_r^2-1}{n_r^2+2}$ and vacuum permittivity ϵ_0. The total electric field consists of the trap ($\mathbf{E}_{tr}(\mathbf{R})$), cavity ($\mathbf{E}_{cav}(\mathbf{R})$) and free space electromagnetic modes ($\mathbf{E}_{free}(\mathbf{R})$) yielding the interaction Hamiltonian

$$\hat{H}_{int} = -\frac{1}{2}\alpha[\mathbf{E}_{tr}(\mathbf{R}) + \mathbf{E}_{cav}(\mathbf{R}) + \mathbf{E}_{free}(\mathbf{R})]^2 \quad (1)$$

$$\approx \hat{H}_{CS} + \hat{H}_{DR} + \hat{H}_{CAV} \quad (2)$$

where $\mathbf{E}_{cav}(\mathbf{R})$ and $\mathbf{E}_{free}(\mathbf{R})$ are only populated by scattering events from the particle ($n_{trap} \gg n_{cav}$ with n_{trap} (n_{cav}) being the number of trap (cavity) photons). As can be seen from Eq. (1), the interaction Hamiltonian consists of six terms of which only the two terms proportional to $\mathbf{E}_{tr}(\mathbf{R})\mathbf{E}_{cav}(\mathbf{R})$ and $\mathbf{E}_{cav}(\mathbf{R})^2$ are relevant for the following discussion[36]. The former one gives rise to the opto-mechanical coupling by CS, and the latter to the coupling achieved by actively driving the cavity. The term $\propto \mathbf{E}_{tr}^2(\mathbf{R})$ gives rise to the trapping potential, while the term $\propto \mathbf{E}_{tr}(\mathbf{R})\mathbf{E}_{free}(\mathbf{R})$ causes recoil

heating[36,41], which can be neglected for the moderate vacuum conditions presented here[7,41]. The remaining two terms can be safely neglected according to ref. [36].

In the following, we use the simplified interaction Hamiltonian given by Eq. (2) where we separate the parts contributing to the optomechanical coupling due to CS $\hat{H}_{CS}$, active driving $\hat{H}_{DR}$, and population of the intracavity field $\hat{H}_{CAV}$ (see "Interaction Hamiltonian and power spectral densities" section).

For the measurements presented here, the trap is x-polarised with $\theta = 0$ (see inset Fig. 1). This simplifies $\hat{H}_{CS}$ to $\hat{H}_{CS} = -\hbar[g_y(\hat{a}^\dagger + \hat{a})(\hat{b}_y^\dagger + \hat{b}_y) + g_z(\hat{a}^\dagger - \hat{a})(\hat{b}_z^\dagger + \hat{b}_z)]$, where $\hat{a}$ ($\hat{a}^\dagger$) is the photon annihilation (creation) operator and $\hat{b}$ ($\hat{b}^\dagger$) is the phonon annihilation (creation) operator. The CS optomechanical coupling strengths $g_{y,z}$ are

$$\begin{bmatrix} g_y \\ g_z \end{bmatrix} = \frac{1}{2} \begin{bmatrix} G_\perp k_c y_{zpf} \sin\phi \\ -i\, G_\perp k_t z_{zpf} \cos\phi \end{bmatrix} \quad (3)$$

with cavity wavevector $k_c = 2\pi/\lambda_c$, zero-point fluctuations $y_{zpf}, z_{zpf} = \sqrt{\frac{\hbar}{2m\Omega_{y,z}}}$ and $\phi = 2\pi y_0/\lambda_c$, with y_0 being the particle position along the cavity axis and $y_0 = \lambda_c/4$ corresponding to the intensity minimum.

The optical cavity resonance frequency shift caused by a particle located at maximum intensity of the intracavity standing wave is $G_\perp = \alpha E_0 \sqrt{\frac{\omega_c}{2\hbar\epsilon_0 V_c}}$ with cavity mode volume $V_c = \pi w_c^2 L_c/4$, cavity waist w_c, cavity length L_c, and $\omega_c = 2\pi c/\lambda_c$. The trap electric field is $E_0 = \sqrt{\frac{4P_t}{\pi\epsilon_0 c w_x w_y}}$ with trap waists w_x and w_y.

Due to the intracavity standing wave, the optomechanical coupling strength has a sinusoidal dependence on y_0 with opposite phase for g_y and g_z. In contrast, $g_x = 0$ if $\theta = 0$.

For clarity, we limit the discussion to coupling along the cavity axis (y), such that $\Omega_m = \Omega_y$ and $g = g_y$. Similar results can be obtained for the other directions x, z with the same level of control.

The maximum expected coupling strength from CS is $g_y^{max} = G_\perp k_c y_{zpf} = 2\pi \times 31.7$ kHz for our parameters. However, we displace the particle by $\delta z \approx 40\,\mu m$ from the cavity centre for better experimental stability. Hence, our expected optomechanical coupling strength is reduced by $\approx 30\%$ down to $g_y^{th} = 2\pi \times 22.6$ kHz, enabling the SCR with $g_y > \kappa$. Despite the fact that this value is a factor of ≈ 3 lower than previously reported[9], the deep SRC with $g > \kappa$ remains unaccomplished.

Transition to the SCR. In the weak coupling regime $g < \kappa$, the Lorentzian-shaped spectra of our mechanical oscillator displays a single peak at its resonance frequency Ω_m. When g increases, the energy exchange rate between optical and mechanical mode grows until the SCR is reached at $g > \kappa/4$ (ref. [33]). In the SCR, the optical and mechanical mode hybridise, which gives rise to two new eigenmodes at shifted eigenfrequencies $\Omega_\pm$ (see Eq. (9)). At this point, the energy exchange in between the optical and mechanical mode is faster than the decoherence rate of each individual mode. The hybridised eigenmode frequencies

$$\Omega_\pm = \Omega_m - \frac{\Omega_m + \Delta}{2} \pm \sqrt{g_y^2 + \left(\frac{\Omega_m + \Delta}{2}\right)^2} \quad (4)$$

experience an avoided crossing, the so-called NMS, which reaches a maximum of $\Omega_+ - \Omega_- = 2g_y$ at the optimal detuning $\Delta = -\Omega_m$. The linewidth of the hybrid modes at this detuning is $(\kappa + \Gamma_m)/2$.

Therefore, Γ_m needs to be smaller or comparable to κ to resolve the NMS of $2g_y$.

As can be seen from Eq. (3), we control g_y through various parameters like the trap power P_t, the particle position y_0 and the polarisation angle θ. The optical coupling rate Γ_{opt} depends additionally on the trap detuning Δ and is maximised at $\Delta = -\Omega_m$ to $\Gamma_{opt} = 4g_y^2/\kappa$ (refs. [7,12]). While P_t and Δ only influence the magnitude of the coupling strength, y_0 and θ change also the nature of the coupling from 1D to potentially 3D[36]. For simplicity, we focus on varying Δ and y_0 in the following measurements and keep P_t, θ and $\Gamma_m = 2\pi \times 0.8$ kHz, corresponding to $p = 1.4$ mBar, fixed (see "Experimental setup" section). The range of Δ is limited due to instabilities in the experiment.

Observation of strong coupling. Figure 2 left panel displays the experimental position power spectral density (PSD) versus Δ for different y_0. Throughout the remaining part of the manuscript, we fit our PSD to Eq. (9), if not stated differently. From this fit, we can extract the hybridised modes $\Omega_\pm$ that are separated by $2g_y$. We cover a total distance of $\delta y_0 \approx \lambda_c/4$ and change the optomechanical coupling strength, and therefore also the NMS, from (a) $g_y/2\pi = 22.8$ kHz, (b) 15.4 kHz, (c) 4.6 kHz and (d) 0 kHz, exploring the entire range from strong coupling to zero coupling. The right panel shows the fit, which is in good agreement with the data. We observe two eigenmodes $\Omega_\pm$ with an exceptional NMS of $2g_y \approx 4.6\kappa$ at $\Delta = -\Omega_m$, corresponding to 20% of the bare mechanical eigenfrequency, once the system enters the SCR at $g > \kappa/4$ (ref. [33]). For $g_y = 0$, we observe only the mechanical mode with slightly increased frequency $\Omega_m = 2\pi \times 200$ kHz due to the additional trapping potential supplied by the cavity field (see Fig. 2d). In Fig. 2a and b, we observe an additional NMS in the y-mode, which stems from a second cross polarised optical mode. Note that, throughout all our measurements (see Figs. 2–4), the second NMS is the largest source for discrepancies between experiment and theory (for more details, see Supplementary Information). We also attribute the NMS of the x-mode at $\Omega/\Omega_m = 0.89$ to the second optical mode as observed in Fig. 2d, since the x-mode should be decoupled from the first mode ($g_x = 0$ if $\theta = 0$).

Figure 3a–c displays the particle's position PSD at different Δ while it is located at the intensity minimum, corresponding to the position of maximum coupling $g_y = 2.3\kappa$, displayed in Fig. 2a. Our theory (yellow) captures the data (purple) well. In Fig. 3a, the optical mode and mechanical mode begin to hybridise into new eigenmodes at $\Delta = -1.5\Omega_m$ which is confirmed by a second peak appearing at $\Omega \approx 2\pi \times 300$ kHz. The hybridisation becomes stronger as Δ approaches the cavity resonance and the NMS is maximised at $\Delta \approx -\Omega_m$ as shown in Fig. 3c. The dependence of the new eigenmodes $\Omega_\pm$ on Δ is shown in Fig. 3d, displaying clearly the expected avoided crossing of $2g_y$. The solid line is a fit to Eq. (4). The edges of the shaded area represent the upper and lower limit of the fit, which we obtain by fitting only the upper branch (yellow) or the lower branch (purple), respectively.

As already discussed previously, our experiment allows to change the optomechanical coupling by changing various experimental parameters, which stands in contrast to many other experimental platforms. Figure 4 displays this flexibility to reach the SCR by demonstrating the position dependence of g_y at optimal detuning $\Delta \approx -\Omega_m$ extracted from the data Fig. 2a–d. The experimental and theoretical position PSDs versus y_0 are depicted in Fig. 4a and b. The mode at $\Omega/\Omega_m \approx 0.89$ corresponds to the decoupled x-mode. The dashed line highlights the theoretical frequency of the eigenmodes $\Omega_\pm/\Omega_m$ following Eq. (4). In both experiment and theory, we observe the expected sinusoidal behaviour predicted by Eq. (3). Figure 4c depicts
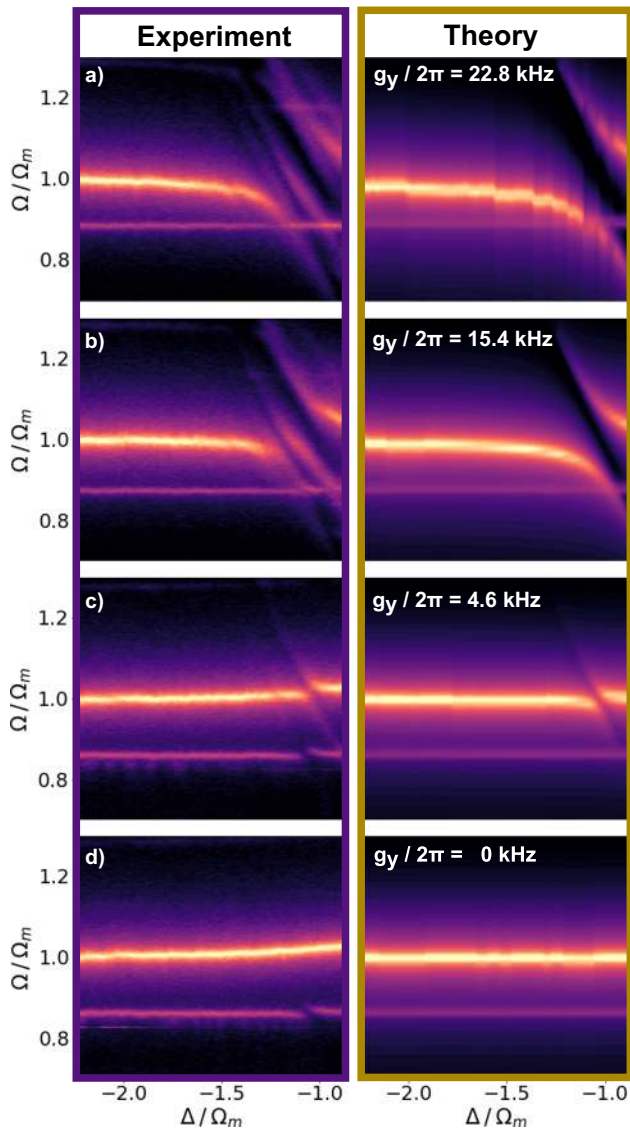
Experiment	Theory

Fig. 2 Normal mode splitting. Particle's position power spectral density PSD(Ω) versus Δ for different y_0 and therefore various g_y. Experimental data are displayed on the left, and theory on the right. The bare mechanical (optical) modes correspond to horizontal (diagonal) lines. **a** Maximum normal mode splitting of $2g_y$ is observed at $\Delta = -\Omega_m$ yielding a value of $g_y = 2\pi \times 22.8$ kHz $= 2.3\kappa$, where $y_0 \approx \lambda_c/4$ is close to the intensity minimum (see Eq. (3)). **b** When the particle is moved by $\delta y_0 \approx 0.12\lambda_c$, the coupling reduces to $g_y = 2\pi \times 15.4$ kHz $= 1.5\kappa$. **c** Normal mode splitting is still visible at $\delta y_0 \approx 0.2\lambda_c$, yielding $g_y = 2\pi \times 4.6$ kHz $= 0.46\kappa$. **d** At the intensity maximum, corresponding to a shift of $\delta y_0 \approx \lambda_c/4$ and $g_y = 0$ kHz, the normal mode splitting vanishes and we only see a shift of $\delta\Omega_m \approx 2\pi \times 5$ kHz in the mechanical frequency due to the increased intracavity photon number (see Supplementary Fig. 1). In general, we observe a good agreement between experimental data and theory. We attribute discrepancies to a second cross polarised cavity mode inducing a second normal mode splitting (for more details, see Supplementary Information).

$|g_y| = (\Omega_+ - \Omega_-)/2$ (circles) extracted from Fig. 4a. The dashed line represents the fit to the absolute value of Eq. (3) yielding $g_y^{exp} = 2\pi \times (22.8 \pm 0.2)$kHz which coincides well with the theoretical value of $g_y^{th} = 2\pi \times 22.6$ kHz. The measured period coincides with the expected period of $\lambda_c/4$. The shaded area corresponds to $3\sigma_{std}$ of the fit.

Discussion

As a figure of merit to assess the potential of our system for quantum applications, we use the quantum cooperativity, which yields here $C_{CS} = (2g_y^{max})^2/(\kappa\Gamma_m(n_{th}+1)) = 8\times 10^{-6}$ at a pressure $p = 1.4$ mbar and promises a value as large as $C_{CS} \approx 36$ at $p = 3 \times 10^{-7}$ mbar, since $\Gamma_m \propto p$. At this low pressure, the photon recoil heating rate Γ_{rec}[41] equals our mechanical decoherence rate $\Gamma_m(n_{th}+1)$, and therefore halves the reachable C_{CS}. The maximum C_{CS} is ultimately limited by Γ_{rec}, regardless if we reduce the pressure even further. Nevertheless, this predicted value of C_{CS} is many orders of magnitude larger than what has been achieved in levitation setups by actively driving the cavity[7,24] and larger than achieved in ref. [9]. More importantly it enables coherent quantum control at $g \gg \kappa, \Gamma_m \cdot n_{th}$ at pressure levels $p \leq 10^{-6}$ mbar, a pressure regime commonly demonstrated in numerous levitation experiments[7,9,41].

Furthermore, our experimental parameters promise the possibility of motional ground state cooling in our system[9], which in combination with coherent quantum control enables us to fully enter the quantum regime with levitated systems and to create non-classical states of motion and superposition states of macroscopic objects in free fall experiments[10,11] in the future.

Methods

Experimental setup. The experimental setup is displayed in Fig. 5. A silica nanoparticle is loaded at ambient pressure into a long range single beam trap and transferred to a more stable, short range optical tweezers trap[42] (with wavelength $\lambda_t = 1064$ nm, power $P \simeq 150$ mW, focusing lens NA = 0.8) inside a vacuum chamber. Due to the tight focusing, the nanoparticle non-degenerate eigenfrequencies are $\Omega_{x,y,z} = 2\pi \times$ (172 kHz, 197 kHz, 56 kHz), respectively. The optical tweezers are mounted on a 3D nanometre resolution piezo stage allowing for precise 3D positioning inside a high finesse Fabry-Perot cavity (with cavity finesse $F = 540,000$, free spectral range FSR $= 2\pi \times 5.4$ GHz).

In order to control the detuning $\Delta = \omega_t - \omega_c$ between the cavity resonance ω_c and the trap field ω_t, we use a weak cavity field for locking the cavity via the Pound-Drever-Hall (PDH) technique on the TEM01 mode minimising additional heating effects through the photon recoil heating of the cavity lock field. The PDH errorsignal acts on the internal laser piezo and an external AOM (not shown). We separate lock and trap light in frequency space by one free spectral range (FSR) such that the total detuning between lock and trap yields $\omega_t = \omega - FSR - \Delta$. The variable EOM modulation $FSR + \Delta$ is provided by a signal generator. The intracavity power can be deduced from the transmitted cooling light observed on a photodiode behind the cavity (CO).

All particle information shown is gained in forward balanced detection interfering the scattered light field and the non-interacting part of the trap beam as shown in Fig. 5. The highly divergent trap light is collected using a lens (NA = 0.8). We use three balanced detectors (FS) to monitor the oscillation of the particle in all three degrees of freedom.

The data time traces are acquired at 1 MHz acquisition rate. Each particle position PSD is obtained by averaging over $N = 25$ samples of which each one is calculated from individual 40 ms time traces, corresponding to a total measurement time of $t = 1$ s.

We keep the pressure stable at $p = 1.4$ mbar. The thermal bath couples as

$$\Gamma_m = \frac{k_B T}{\hbar Q_m n_{th}} = 15.8 \frac{R^2 p}{m v_{gas}} \qquad (5)$$

where $Q_m = \Omega_m/\Gamma_m$ is the mechanical quality factor, $n_{th} = \frac{k_B T}{\hbar \Omega_m}$ the thermal occupation number, R the particle radius, p the surrounding gas pressure and $v_{gas} = \sqrt{3k_B T/m_{gas}}$.

In the measurements presented, we cool our particle's centre of mass motion to $T = 235$, corresponding to a reduction of the phonon occupation by roughly 20%. The theoretically expected heating rate due to the residual gas accounts fully for the experimentally observed heating rate.

Interaction Hamiltonian and power spectral densities. Following ref. [36], the relevant contributions to the CS interaction Hamiltonian for $\theta = 0$ are given by

$$\frac{\hat{H}_{CS}}{\hbar} = -g_y(\hat{a}^\dagger + \hat{a})(\hat{b}_y^\dagger + \hat{b}_y)$$
$$-g_z(\hat{a}^\dagger - \hat{a})(\hat{b}_z^\dagger + \hat{b}_z) \qquad (6)$$
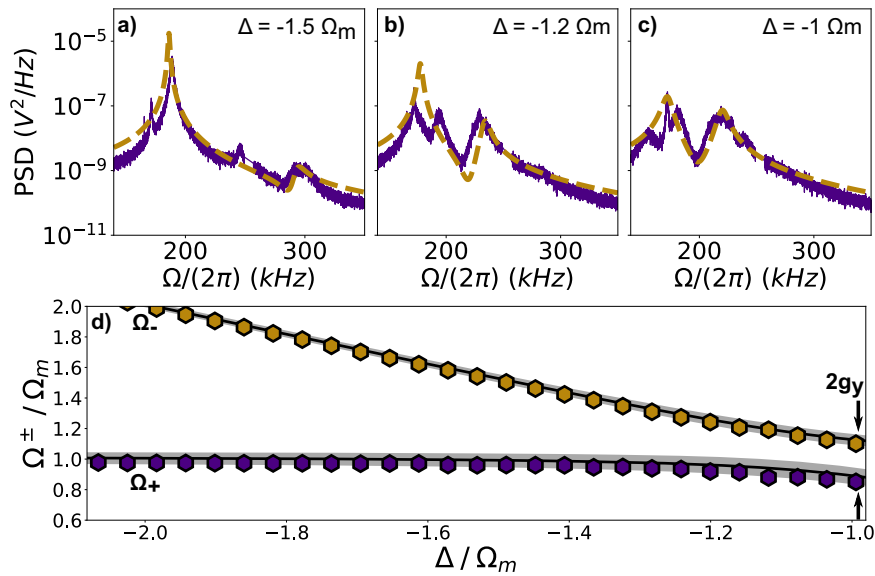
Fig. 3 Power spectral density versus cavity detuning Δ. a–c Experiment (purple) and theory (yellow, dashed) fitted to Eq. (9) at $\Delta = -2\pi \times 293\,\text{kHz} \approx -1.5\Omega_m$ (**a**), $\Delta = -2\pi \times 225\,\text{kHz} \approx -1.2\Omega_m$ (**b**) and $\Delta = -2\pi \times 205\,\text{kHz} \approx -\Omega_m$ (**c**). The optomechanical coupling strength g_y grows with increasing Δ. Optical and mechanical modes start to hybridise clearly at $\Delta \geq -1.5\Omega_m$. We attribute the discrepancy between data and theory to the second optical mode (see Supplementary Informtation). **d** Hybridised eigenmodes $\Omega_\pm$ versus Δ at the intensity minimum ($y_0 \approx \lambda_c/4$). Maximum normal mode splitting of $2g_y$ with $g_y = 2\pi \times 22.8\,\text{kHz} = 2.3\kappa$ occurs at $\Delta = -\Omega_m$. The black line fits the data to Eq. (4), while the inner (outer) edges of the grey area correspond to a fit using solely to the upper (lower) branch Ω_- (Ω_+).
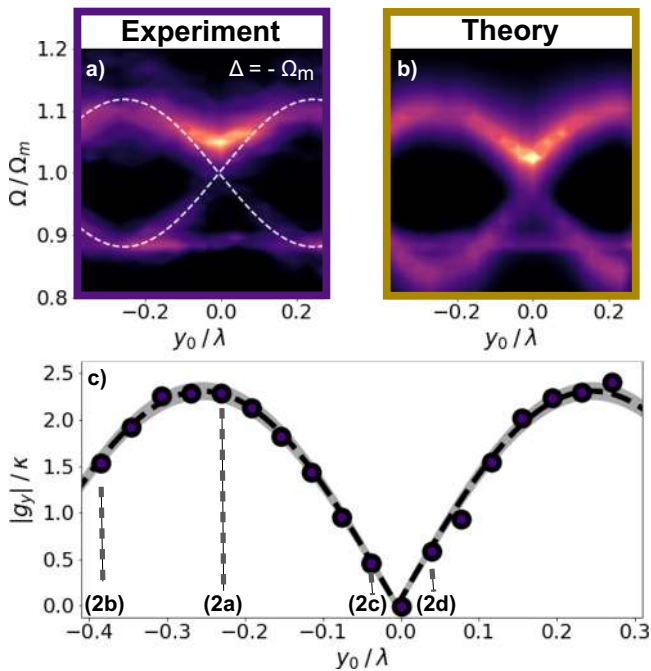
Fig. 4 Normal mode splitting versus particle position y_0. a Experiment and **b** theory according to Eq. (9). Particle position power spectral density PSD(Ω) at the optimal $\Delta = -2\pi \times 193\,\text{kHz} \approx -\Omega_m$ along y_0 is shown. The hybridised modes split by $2g_y$. The white dashed line displays $\Omega_\pm/\Omega_m = 1 \pm g_y/\Omega_m$ where g_y follows Eq. (3). The mechanical mode at $\Omega/\Omega_m \approx 0.89$ corresponds to the mechanical x-mode. The data and fit show very good agreement. **c** $|g_y|$ at $\Delta \approx -\Omega_m$ versus y_0. Maximum and minimum coupling are separated by $\delta y_0 = \lambda_c/4$ as expected by Eq. (3). Black dashed line fits to the absolute value of Eq. (3) with a maximum $g_y^{\max} \approx -2.3\kappa$ and the grey shaded area corresponds to $3\sigma_{\text{std}}$ of the fit. The dotted lines indicate the positions used in Fig. 2.
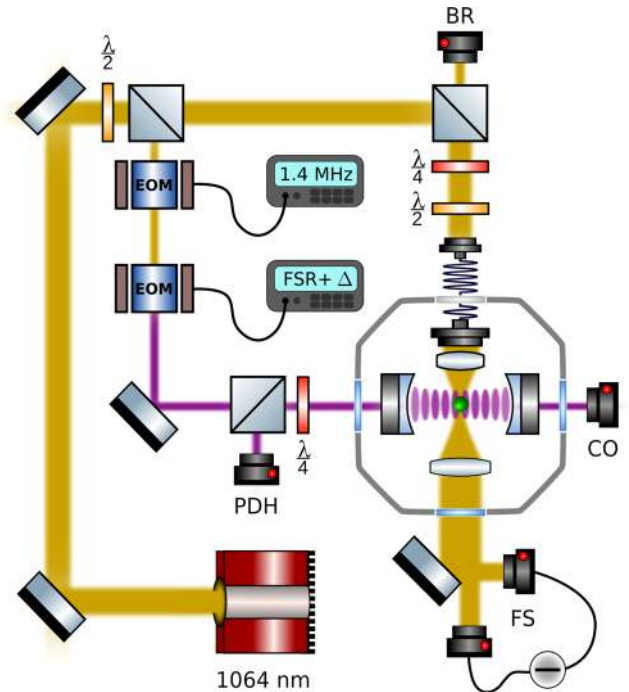
Fig. 5 Extended experimental setup. A 1064 nm Mephisto laser (yellow) traps a silica particle of $d = 177\,\text{nm}$ inside a high finesse cavity (purple). The trap light is locked at a variable detuning $\Delta + $ FSR from the cavity resonance via the Pound-Drever-Hall technique by detecting the error signal on a photodiode (PDH). The particle motion is detected in backreflection (BR) and balanced forward detection (FS). The intracavity field is estimated from the transmitted power detected on a photodiode (CO).

$$\frac{\hat{H}_{\mathrm{DR}}}{\hbar} = -g_y^{\mathrm{dr}}\,\hat{a}^\dagger \hat{a}\,(\hat{b}_y^{\,\dagger} + \hat{b}_y) \tag{7}$$

$$\frac{\hat{H}_{\mathrm{CAV}}}{\hbar} = -\frac{G_\perp}{2}(\hat{a}^\dagger + \hat{a})\cos\phi \tag{8}$$

The single photon optomechanical coupling strength achieved by actively driving the cavity is $g_y^{\mathrm{dr}} = \frac{\alpha\omega_c}{2\epsilon_0 V_c} k_c y_{\mathrm{zpf}} \sin(2\phi) = 2\pi \times 0.05\,\mathrm{Hz}\sin(2\phi)$. This value is enhanced by the intracavity photon number $n_{\mathrm{cav}} = 1.6 \times 10^8$, inferred from the transmitted cavity power P_{out}. At optimal conditions, we achieve $g_y^{\mathrm{rp}}\sqrt{n_c} = 2\pi \times 0.6\,\mathrm{kHz}$. Thus, the optomechanical coupling strength is about 40 times larger for CS, since the photons contributing to the CS interaction are confined in a much smaller volume due to the much smaller trap waist $w_t \times w_c \ll w_c^2$.

The mechanical susceptibility χ is given as[33]

$$|\chi(\Omega)|^2 = \frac{1}{m^2[(\Omega_m^2 + 2\Omega\delta\Omega_m(\Omega) - \Omega^2)^2 + (\Omega\Gamma_{\mathrm{eff}}(\Omega))^2]} \tag{9}$$

$$\Gamma_{\mathrm{eff}}(\Omega) = \Gamma_{\mathrm{m}} + \Gamma_{\mathrm{opt}}(\Omega) \tag{10}$$

$$\delta\Omega_m(\Omega) = g_y^2\frac{\Omega_m}{\Omega}\left[\frac{\Delta + \Omega}{(\Delta + \Omega)^2 + \kappa^2/4} + \frac{\Delta - \Omega}{(\Delta - \Omega)^2 + \kappa^2/4}\right] \tag{11}$$

$$\Gamma_{\mathrm{opt}}(\Omega) = g_y^2\frac{\Omega_m}{\Omega}\left[\frac{\kappa}{(\Delta + \Omega)^2 + \kappa^2/4} - \frac{\kappa}{(\Delta - \Omega)^2 + \kappa^2/4}\right] \tag{12}$$

with the effective (optical) damping Γ_{eff} (Γ_{opt}) and the optomechanical spring effect $\delta\Omega_m$. We fit the three mechanical modes $\Omega_{x,y,z}$ to Eq. (9) where g_y, κ, Γ_{m} and the relative mode amplitudes are chosen as free fit parameters.

Data availability
The data that support the findings of this study are available from the corresponding author upon request.

References
1. Chang, D. E. et al. Cavity opto-mechanics using an optically levitated nanosphere. *Proc. Natl Acad. Sci. USA* **07**, 1005–1010 (2010).
2. Romero-Isart, O., Juan, M. L., Quidant, R. & Cirac, J. I. Toward quantum superposition of living organisms. *N. J. Phys.* **12**, 033015 (2010).
3. Kiesel, N. et al. Cavity cooling of an optically levitated submicron particle. *Proc. Natl Acad. Sci. USA* **110**, 35 (2013).
4. Asenbaum, P., Kuhn, S., Nimmrichter, S., Sezer, U. & Arndt, M. Cavity cooling of free silicon nanoparticles in high vacuum. *Nat. Commun.* **4**, 2743 (2013).
5. Millen, J., Fonseca, P. Z. G., Mavrogordatos, T., Monteiro, T. S. & Barker, P. F. Cavity cooling a single charged levitated nanosphere. *Phys. Rev. Lett.* **114**, 123602 (2015).
6. Fonseca, P. Z. G., Aranas, E. B., Millen, J., Monteiro, T. S. & Barker, P. F. Nonlinear dynamics and strong cavity cooling of levitated nanoparticles. *Phys. Rev. Lett.* **117**, 173602 (2016).
7. Meyer, N. et al. Resolved-sideband cooling of a levitated nanoparticle in the presence of laser phase noise. *Phys. Rev. Lett.* **123**, 1–6 (2019).
8. Delić, U. et al. Cavity cooling of a levitated nanosphere by coherent scattering. *Phys. Rev. Lett.* **122**, 123602 (2019).
9. Delić, U. et al. Cooling of a levitated nanoparticle to the motional quantum ground state. *Science* **367**, 892–895 (2020).
10. Romero-Isart, O. et al. Large quantum superpositions and interference of massive nanometer-sized objects. *Phys. Rev. Lett.* **107**, 020405 (2011).
11. Bateman, J., Nimmrichter, S., Hornberger, K. & Ulbricht, H. Near-field interferometry of a free-falling nanoparticle from a point-like source. *Nat. Commun.* **5**, 1–5 (2014).
12. Aspelmeyer, M., Kippenberg, T. J. & Marquardt, F. Cavity optomechanics. *Rev. Mod. Phys.* **86**, 1391–1452 (2014).
13. Millen, J., Monteiro, T. S., Pettit, R. & Vamivakas, A. N. Optomechanics with levitated particles. *Rep. Prog. Phys.* **83**, 026401 (2020).
14. Hempston, D. et al. Force sensing with an optically levitated charged nanoparticle. *Appl. Phys. Lett.* **111**, 133111 (2017).
15. Arita, Y., Mazilu, M. & Dholakia, K. Laser-induced rotation and cooling of a trapped microgyroscope in vacuum. *Nat. Commun.* **4**, 2374 (2013).
16. Kuhn, S. et al. Optically driven ultra-stable nanomechanical rotor. *Nat. Commun.* **8**, 1670 (2017).
17. Monteiro, F., Ghosh, S., van Assendelft, E. C. & Moore, D. C. Optical rotation of levitated spheres in high vacuum. *Phys. Rev. A* **97**, 051802(R) (2018).
18. Reimann, R. et al. GHz rotation of an optically trapped nanoparticle in vacuum. *Phys. Rev. Lett.* **121**, 033602 (2018).
19. Hebestreit, E., Frimmer, M., Reimann, R. & Novotny, L. Sensing static forces with free-falling nanoparticles. *Phys. Rev. Lett.* **121**, 063602 (2018).
20. Rondin, L. et al. Direct measurement of Kramers turnover with a levitated nanoparticle. *Nat. Nanotechnol.* **12**, 1130–1134 (2017).
21. Marshall, W., Simon, C., Penrose, R. & Bouwmeester, D. Towards quantum superpositions of a mirror. *Phys. Rev. Lett.* **91**, 13 (2003).
22. Kleckner, D. et al. Creating and verifying a quantum superposition in a micro-optomechanical system. *N. J. Phys.* **10**, 095020 (2008).
23. Windey, D. et al. Cavity-based 3D cooling of a levitated nanoparticle via coherent scattering. *Phys. Rev. Lett.* **122**, 123601 (2019).
24. Delić, U. et al. Levitated cavity optomechanics in high vacuum. *Quantum Sci. Technol.* **5**, 025006 (2020).
25. Safavi-Naeini, A. H. et al. Squeezed light from a silicon micromechanical resonator. *Nature* **500**, 185–189 (2013).
26. Riedinger, R. et al. Non-classical correlations between single photons and phonons from a mechanical oscillator. *Nature* **530**, 313–316 (2016).
27. Riedinger, R. et al. Remote quantum entanglement between two micromechanical oscillators. *Nature* **556**, 473–477 (2018).
28. Chen, J., Rossi, M., Mason, D. & Schliesser, A. Entanglement of propagating optical modes via a mechanical interface. *Nat. Commun.* **11**, 943 (2020).
29. Gröblacher, S., Hammerer, K., Vanner, M. R. & Aspelmeyer, M. Observation of strong coupling between a micromechanical resonator and an optical cavity field. *Nature* **460**, 724–727 (2009).
30. Teufel, J. D. et al. Circuit cavity electromechanics in the strong-coupling regime. *Nature* **471**, 204–208 (2011).
31. Teufel, J. D. et al. Sideband cooling of micromechanical motion to the quantum ground state. *Nature* **475**, 359–363 (2011).
32. Verhagen, E., Deléglise, S., Weis, S., Schliesser, A. & Kippenberg, T. J. Quantum-coherent coupling of a mechanical oscillator to an optical cavity mode. *Nature* **482**, 63–67 (2012).
33. Dobrindt, J. M., Wilson-Rae, I. & Kippenberg, T. J. Parametric normal-mode splitting in cavity optomechanics. *Phys. Rev. Lett.* **101**, 1–4 (2008).
34. Thompson, R. J., Rempe, G. & Kimble, H. J. Observation of normal-mode splitting for an atom in an optical cavity. *Phys. Rev. Lett.* **68**, 1132–1135 (1992).
35. Vuletić, V., Chan, H. W. & Black, A. T. Three-dimensional cavity Doppler cooling and cavity sideband cooling by coherent scattering. *Phys. Rev. A* **64**, 033405 (2001).
36. Gonzalez-Ballestero, C. et al. Theory for cavity cooling of levitated nanoparticles via coherent scattering: master equation approach. *Phys. Rev. A* **100**, 013805 (2019).
37. Chikkaraddy, R. et al. Single-molecule strong coupling at room temperature in plasmonic nanocavities. *Nature* **535**, 127–130 (2016).
38. Kleemann, M. E. et al. Strong-coupling of WSe2 in ultra-compact plasmonic nanocavities at room temperature. *Nat. Commun.* **8**, 1296 (2017).
39. Gieseler, J. Dynamics of Optically Levitated Nanoparticles in High Vacuum. Ph.D. thesis, ICFO (2014).
40. Tebbenjohanns, F., Frimmer, M., Jain, V., Windey, D. & Novotny, L. Motional sideband asymmetry of a nanoparticle optically levitated in free space. *Phys. Rev. Lett.* **124**, 13603 (2020).
41. Jain, V. et al. Direct measurement of photon recoil from a levitated nanoparticle. *Phys. Rev. Lett.* **116**, 243601 (2016).
42. Mestres, P. et al. Cooling and manipulation of a levitated nanoparticle with an optical fiber trap. *Appl. Phys. Lett.* **107**, 151102 (2015).

Author contributions
A.d.l.R.S. performed the measurements, N.M. evaluated the data and wrote the manuscript, R.Q. supervised the study.

Competing interests
The authors declare no competing interests.

Additional information

Supplementary information is available for this paper at https://doi.org/10.1038/s41467-020-20419-2.

Correspondence and requests for materials should be addressed to N.M.

Peer review information *Nature Communications* thanks James Millen and the other anonymous reviewer(s) for their contribution to the peer review of this work.

Reprints and permission information is available at http://www.nature.com/reprints

Publisher's note Springer Nature remains neutral with regard to jurisdictional claims in published maps and institutional affiliations.